



Numerical simulation study on shear resistance of anchorage joints considering tensile–shear fracture criterion of 2G-NPR bolt

Shulin Ren^{1,2} · Zhigang Tao^{1,2} · Manchao He^{1,2} · Mengnan Li^{1,2} · Qiru Sui^{1,2}

Received: 10 May 2023 / Revised: 27 July 2023 / Accepted: 3 August 2023
© The Author(s) 2023

Abstract

2G-NPR bolt (the 2nd generation Negative Poisson's Ratio bolt) is a new type of bolt with high strength, high toughness and no yield platform. It has significant effects on improving the shear strength of jointed rock mass and controlling the stability of surrounding rock. To achieve an accurate simulation of bolted joint shear tests, we have studied a numerical simulation method that takes into account the 2G-NPR bolt's tensile–shear fracture criterion. Firstly, the indoor experimental study on the tensile–shear mechanical properties of 2G-NPR bolt is carried out to explore its mechanical properties under different tensile–shear angles, and the fracture criterion of 2G-NPR bolt considering the tensile–shear angle is established. Then, a three-dimensional numerical simulation method considering the tensile–shear mechanical constitutive and fracture criterion of 2G-NPR bolt, the elastoplastic mechanical behavior of surrounding rock and the damage and deterioration of grouting body is proposed. The feasibility and accuracy of the method are verified by comparing with the indoor shear test results of 2G-NPR bolt anchorage joints. Finally, based on the numerical simulation results, the deformation and stress of the bolt, the distribution of the plastic zone of the rock mass, the stress distribution and the damage of the grouting body are analyzed in detail. The research results can provide a good reference value for the practical engineering application and shear mechanical performance analysis of 2G-NPR bolt.

Keywords Anchorage joints · 2G-NPR bolt · Tensile–shear fracture criterion · Shear behavior · Numerical simulation

1 Introduction

The engineering rock mass is affected by frequent geological tectonic movement and complex stress field, which often produces many weak structural planes such as fissures, joints and faults. The integrity and continuity of rock mass are seriously damaged by these weak structural planes. The rock mass is easy to produce large deformation and failure phenomena such as dislocation and separation along the weak structural plane, which is also the decisive factor leading to the failure of the anchoring support system (Li et al. 2010a; Ma et al. 2019; Zhang et al. 2022). Field engineering and laboratory tests show that, the fracture of supporting materials are often manifested as a tensile–shear composite failure

mode in which unstable rock mass slips along the structural plane (Li et al. 2010b; Li et al. 2015; Liu et al. 2017; Zheng et al. 2021). Therefore, it is of great significance to carry out research on the shear resistance of bolt anchorage for the stability control of geotechnical engineering.

Indoor anchorage shear test is the main method to study the shear performance of bolt anchorage. The shear mechanics experiment of bolt anchorage granite jointed rock mass was first carried out by Bjurström (Bjurström 1974), the results show that the anchorage angle has a significant effect on the shear performance of bolt. In recent years, relevant researchers have carried out a large number of experimental studies on the influence of joint surface roughness (Wu et al. 2018; Chen et al. 2018; Zheng et al. 2021), anchorage angle (Jalalifar et al. 2010; Lin et al. 2014; Li et al. 2019), surrounding rock strength (He et al. 2022; Chen 2014), bolt type (He et al. 2023; Zhang et al. 2022; Wu et al. 2019a; Li et al. 2016; Chen et al. 2015; Grasselli et al. 2005) and other parameters (Wu et al. 2019b; Cui et al. 2020) on the shear performance of anchorage, including the macroscopic deformation and failure characteristics, shear strength and

✉ Zhigang Tao
taozhigang1981@163.com

¹ State Key Laboratory for Geomechanics and Deep Underground Engineering, Beijing 100083, China

² School of Mechanics and Civil Engineering, China University of Mining and Technology, Beijing 100083, China

shear deformation resistance of bolted rock joints. However, laboratory tests are often complicated to operate and microscopic phenomena cannot be monitored. Numerical simulation methods can better compensate for these defects. Based on PFC2D simulation system, Saadat and Taheri (2019) proposed a new viscous contact model, which realized the fracture response of rock, grouting and bolt-grouting interface during shear process. The PFC simulation method was also used by Chen et al. (2022) to study the macroscopic shear behavior and microscopic failure characteristics of single bolt under different rock joint types. Based on the failure theory of rock bolt, Jiang et al. (2022) modified the mechanical model of pile element in FLAC3D program, and revealed the distribution and evolution characteristics of axial force and shear resistance of rock bolt. Jalalifar et al. (2006) analyzed the interaction mechanism between different anchoring agent thickness and anchor-slurry-surrounding rock through indoor double shear test and finite element simulation. It is proved that the increase of surrounding rock strength and bolt preload has a significant improvement on the shear strength of jointed surrounding rock. However, the numerical simulation methods often simplify the anchorage model. For example, the PFC simulation bolt often simplifies the bolt as a cluster unit with rigid performance. In addition, numerical simulation methods such as finite element often use the tensile mechanical parameters of the bolt to simulate, without considering the mechanical parameters and fracture models under different tensile and shear angles (Song et al. 2017; Sing et al. 2020).

The 2G-NPR bolt (the 2nd generation Negative Poisson's Ratio bolt) is a new type of supporting material developed independently (He et al. 2021, 2022). The new bolt has no necking during the static tensile process, and has excellent characteristics of uniform large deformation, disappearance of yield platform and high strength. The yield strength range is 600–1050 MPa, the elongation range is 30%–68%, and the negative Poisson's ratio effect of the material itself is realized (Gu et al. 2021; Tang et al. 2021). The anchorage shear test of 2G-NPR bolt also reflects its excellent characteristics in resisting shear deformation and improving shear strength (He et al. 2022; 2023). The study of 2G-NPR micromechanical mechanism and molecular scale has also achieved some research results, but these mainly belong to the category of materials science and will not be discussed here (Jia et al. 2023). However, the research on the tensile–shear mechanical properties of 2G-NPR bolt and the numerical simulation of bolt shear has not been carried out.

In summary, two aspects of the problem to be solved in this paper, (1) 2G-NPR bolt tensile–shear fracture criterion. (2) Accurate simulation of bolted joint shear test. Firstly, the indoor experimental study on the tensile–shear mechanical properties of 2G-NPR bolt is carried out to explore the mechanical properties under different tensile–shear angles,

and the fracture criterion considering the tensile–shear angle is established. Then, a three-dimensional accurate numerical simulation method considering the tensile–shear mechanical constitutive and fracture criterion of the bolt, the elastoplastic mechanical behavior of surrounding rock and the damage and deterioration of grouting body is proposed, and compared with the indoor shear test results of 2G-NPR bolt anchorage joint. Finally, based on the numerical simulation results, the microscopic information such as the deformation and stress of the bolt, the distribution of the plastic zone of the rock mass, the stress distribution and the damage of the grouting body are analyzed in detail. The research results have good reference value for the practical engineering application of 2G-NPR bolt.

2 Tensile–shear mechanical properties and fracture criterion of 2G-NPR bolt

2.1 Tensile–shear mechanical test of 2G-NPR bolt

The indoor mechanical properties tests under different tensile–shear angles were carried out to study the tensile–shear mechanical properties of 2G-NPR bolt. According to the relevant processing requirements of GB/T 228.1-2010 for standard specimens of steel bar mechanics test and the structure of tensile shear test tooling, 2G-NPR bolt was processed into standard specimens of mechanical test. As shown in Fig. 1a, the standard sample is made of a 2G-NPR bolt with a diameter of 18 mm by cutting, grinding and other processes. The sample gauge is 100 mm and the diameter is 10 mm. In addition, each sample is subjected to at least three tests under the same test conditions to ensure the accuracy of the experimental results. All tests are performed at room temperature and quasi-static conditions.

In order to realize the tension–shear combination test at different angles, a tension–shear clamping device that can meet the requirements of this experiment was made with reference to the relevant experimental design (Song et al. 2020). As shown in Fig. 1b, the device is mainly composed of pull rod, pull plate and sample fixture. The positioning holes with six angles are set on the pull plate, which are 0°, 18°, 36°, 54°, 72° and 90°, respectively. The tensile–shear tests with different angles are realized by connecting different positioning holes, that is, 0° is the pure tensile test, 90° is the pure shear test, and the middle angle corresponds to the tensile–shear combination test. The loading speed of the test sample is controlled by adjusting the loading speed of the test machine. The loading speed of this experiment is 0.5 mm/min to ensure the quasi-static loading. During the experiment, the testing machine can automatically record the test data such as force and displacement.

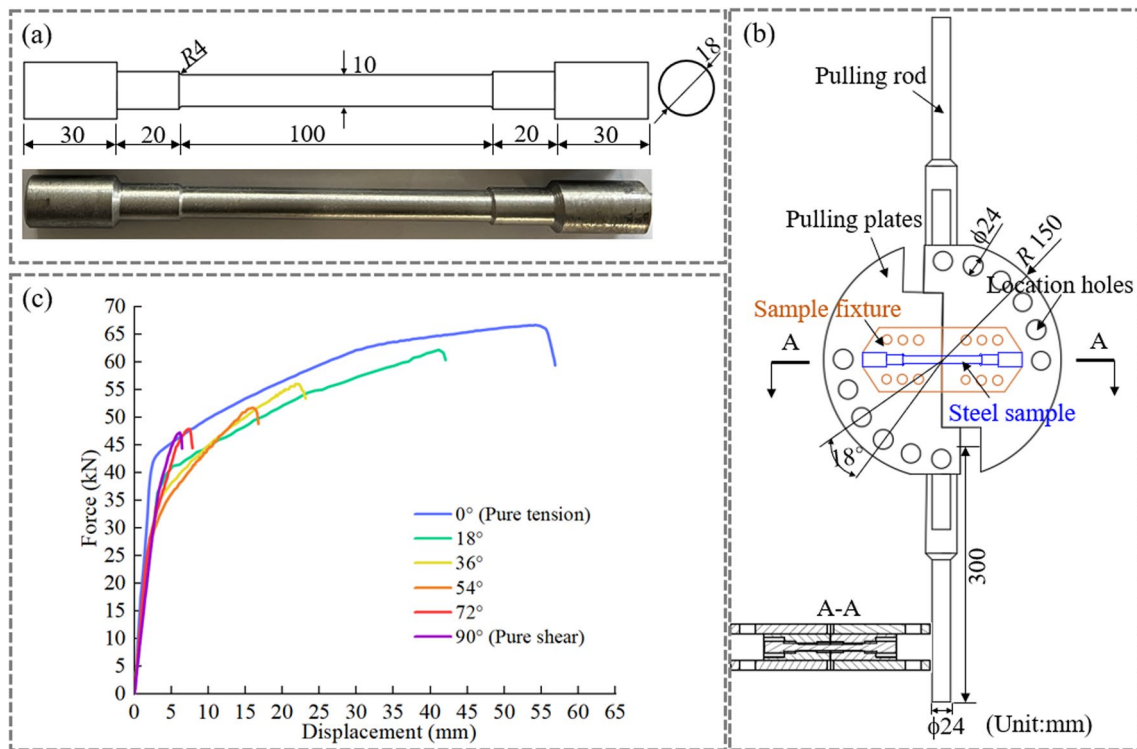


Fig. 1 The combined tensile–shear test of 2G-NPR bolt **a** Geometry of specimens **b** Test setup **c** The force–displacement curves of the combined tensile–shear test

Figure 1c shows the force–displacement curves of 2G-NPR bolt under different tensile–shear test conditions (0°, 18°, 36°, 54°, 72° and 90°). Under pure tensile conditions, the maximum force is 66.727 kN, and the elongation reaches 56.86%, which has significant high ductility and high strength mechanical properties. With the increase of the tensile–shear angle, the deformation and strength of the bolt show a decreasing trend. Under the test condition of the tensile–shear angle of 90°, the sample basically shows the shear brittle fracture characteristics of small deformation. Compared with ordinary steel (He et al. 2021), 2G-NPR steel is significantly different, the curves of 2G-NPR bolt under different tensile–shear angles have no yield platform, and the curves are mainly divided into elastic stage, plastic strengthening stage and fracture failure stage, with quasi-ideal elastoplastic characteristics.

2.2 Tensile–shear fracture criterion of 2G-NPR bolt

Based on the results of indoor mechanical tests, the finite element Abaqus/Explicit numerical analysis method is adopted, and the fracture prediction and failure model of 2G-NPR bolt under tension-shear conditions are studied. Firstly, according to the load–displacement curves obtained from the test, the engineering stress–engineering strain curves are calculated by Eqs. (1) and (2), then the true

stress–true strain curves are calculated on this basis. During the tensile process of the bolt, when the strength reaches the peak load, the specimen will produce necking phenomenon, that is, the cross-sectional area of the bolt does not change evenly (Ling et al. 1996). Therefore, the true stress–true strain data of the 2G-NPR bolt need to be calculated in two parts: before necking and after necking, the true stress–true strain curve before necking is calculated by Eqs. (3) and (4).

$$\epsilon_{eng} = \frac{\Delta l}{l_0} \tag{1}$$

$$\sigma_{eng} = \frac{N}{A_0} \tag{2}$$

$$\epsilon_{true} = \ln(\epsilon_{eng} + 1) \tag{3}$$

$$\sigma_{true} = \sigma_{eng}(\epsilon_{eng} + 1) \tag{4}$$

where Δl represents the deformation length of the specimen, l_0 represents the initial length of the specimen gauge, N is the specimen load, A_0 is the initial cross-sectional area of the specimen.

The scholars have carried out a lot of research on the calculation method of true stress—true strain after necking

(Ling et al. 1996; Song et al. 2020; Gu et al. 2021). In this paper, the weighted average method with simple form and calculation program is used to calculate the true stress-true strain curve data of 2G-NPR bolt after necking. As shown in Fig. 2a, this method assumes the upper and lower bounds of the true stress–true strain curve after necking, and the expressions are Eqs. (5) and (6), respectively. Based on the upper and lower bounds of the curve and the weighted average parameter w , the true stress-true strain expression (Eq. (7)) after necking is established.

$$\sigma_{\text{true}} = \sigma_n \cdot \exp(\epsilon_{\text{true}} - \epsilon_n) \quad (\epsilon > \epsilon_n) \tag{5}$$

$$\sigma_{\text{true}} = \sigma_n (\epsilon_{\text{true}} / \epsilon_n)^{\epsilon_n} \quad (\epsilon > \epsilon_n) \tag{6}$$

$$\sigma_{\text{true}} = \sigma_n [w \cdot \exp(\epsilon_{\text{true}} - \epsilon_n) + (1 - w) \cdot (\epsilon_{\text{true}} / \epsilon_n)^{\epsilon_n}] \quad (\epsilon > \epsilon_n, 0 \leq w \leq 1) \tag{7}$$

where ϵ_n and σ_n are the true strain and true stress at the necking respectively, and w is the weighted average coefficient.

The trial and error method is used to adjust the value of w . Through numerical trial calculation and comparison with the test curves, the optimal weight coefficient w is finally determined. Figure 2b is the result of load-displacement simulation curves under different weight coefficients. Finally, the value of w is selected as 0.4, and the simulation result of the true stress–strain curves corresponding to this parameter is the most consistent with the experimental curves.

Based on the true stress-true strain data of the full loading history, and the fracture displacement of the 2G-NPR bolt in the load–displacement curve is obtained from the indoor test results. The fracture strain value ϵ_f of the

specimen corresponding to the fracture displacement is obtained by finite element numerical analysis. The stress triaxiality η and the equivalent plastic strain curve ϵ_p at the center of the specimen are output at the failure position of the specimen in the numerical calculation model. The average stress triaxiality η_{avg} before the fracture strain ϵ_f is calculated by the Eq. (8) (Zhang et al. 2019). As shown in Table 1, through the calculation of different tensile–shear angle test conditions, the average stress triaxiality and fracture strain of 2G-NPR bolt under different tensile–shear conditions are finally obtained.

$$\eta_{\text{avg}} = \frac{1}{\epsilon_f} \int_0^{\epsilon_f} \eta(\epsilon_p) d\epsilon_p \tag{8}$$

where η_{avg} is the average stress triaxiality, ϵ_f is the fracture strain value, and ϵ_p is the equivalent plastic strain.

The Johnson–Cook failure model (Johnson et al. 1985) takes into account the effects of stress triaxiality, strain rate and temperature on the mechanical properties of materials. Its equation form is simple and the parameters are easy to

Table 1 Average stress triaxiality and fracture strain of 2G-NPR bolt

Tensile–shear test angle (°)	Average stress triaxiality η_{avg}	Fracture strain ϵ_f
0	0.392	1.167
18	0.310	0.565
36	0.260	0.509
54	0.184	0.474
72	0.115	0.417
90	0.002	0.299

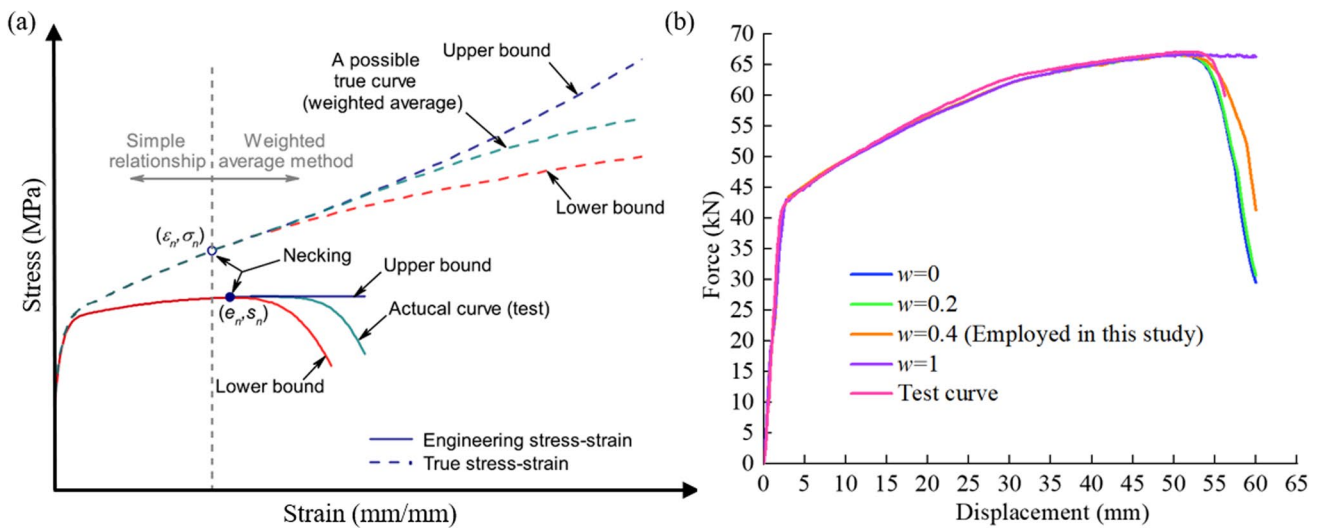


Fig. 2 a Weighted average method (Song et al. 2020) b Weighted average parameter using trial and error method

calibrate (Eq. (9)), and it is also widely used in the prediction of material fracture failure. The model is used to fit the average stress triaxiality and fracture strain to obtain the fracture parameters. Finally, the fracture parameters D_1 , D_2 , D_3 are 0.374, 0.002 and 14.753, respectively.

$$\epsilon_f = [D_1 + D_2 \exp(D_3 \sigma^*)] \tag{9}$$

where, D_1 , D_2 , D_3 are the influence parameters of stress triaxiality; σ^* is the stress triaxiality.

Figure 3 shows the simulation results of 2G-NPR bolt under 0° , 54° and 90° tension-shear angles, including the test result curve, the numerical simulation curve without considering fracture and considering fracture criterion. The results show that the numerical simulation considering fracture criterion can better reflect the mechanical

properties and deformation fracture process of 2G-NPR bolt.

3 2G-NPR bolt anchorage joint shear numerical simulation

The shear process of anchorage rock joint is a complex non-linear process of deformation and failure of bolt, jointed rock mass and grouting body. A large number of anchorage shear laboratory tests of 2G-NPR bolt have been carried out by the author (He et al. 2022; 2023). Based on the relevant experimental basis, a three-dimensional refined numerical simulation method considering the elastic–plastic mechanical behavior of rock mass, the tensile–shear fracture criterion

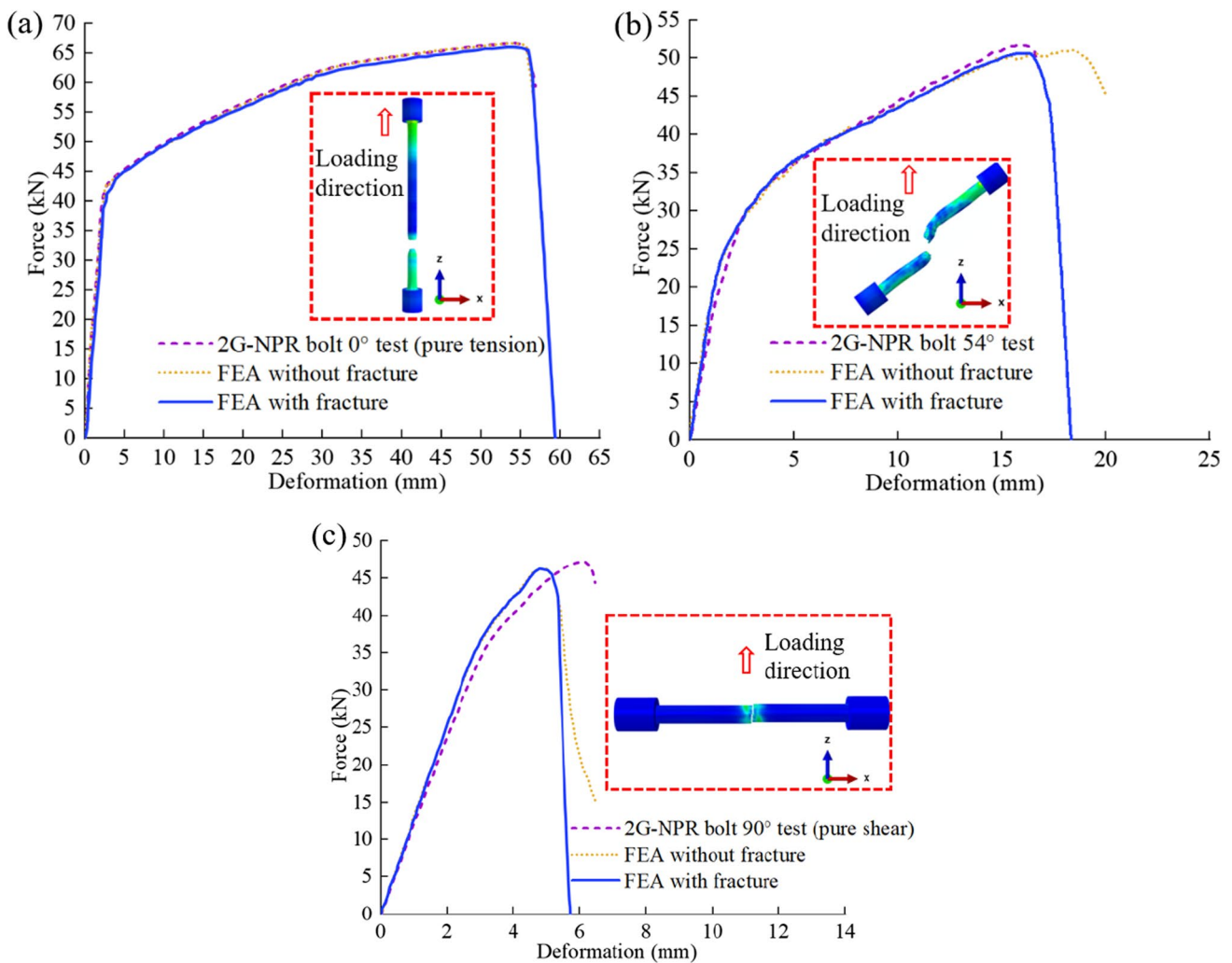


Fig. 3 Comparisons of force–deformation curves and failure modes obtained from tests and FE analysis (with fracture model) at different loading angles: **a** 0° (Pure tension), **b** 54° (Combined tension and shear), and **c** 90° (Pure shear)

of bolt and the damage and deterioration of grouting body is proposed.

3.1 Constitutive model of numerical model of anchored joint

3.1.1 Rock yield criterion

The nonlinear and elastoplastic mechanical properties of rock mass material deformation and failure are fully considered by Mohr–Coulomb model, and the simulation of rock mechanical properties can obtain more accurate results. Therefore, Mohr–Coulomb model is used to simulate rock materials. For the general stress state, the model is more conveniently expressed by three stress invariants:

$$F = R_{mc}q - p \tan \varphi - c = 0 \tag{10}$$

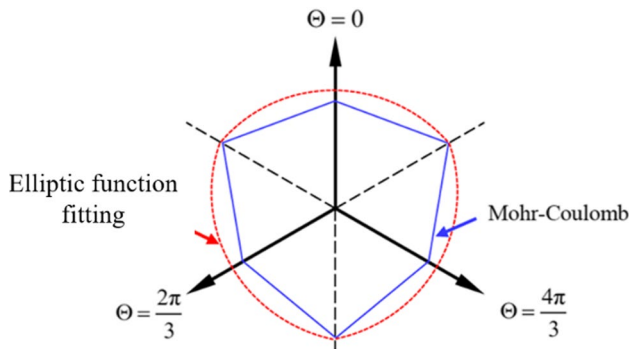


Fig. 4 Plastic potential surface of Mohr-Coulomb model

$$R_{mc} = \frac{1}{\sqrt{3} \cos \varphi} \sin \left(\Theta + \frac{\pi}{3} \right) + \frac{1}{3} \cos \left(\Theta + \frac{\pi}{3} \right) \tan \varphi \tag{11}$$

where q is deviatoric stress; p is the average stress; c is cohesion; R_{mc} is the shape function of the yield surface on the control π plane; Θ is the polar angle.

Figure 4 is the Mohr–Coulomb criterion plastic potential surface. The elliptic function is used as the potential surface to fit the hexagonal section pyramid. The continuous smoothness of the ellipse can effectively ensure its convergence.

3.1.2 Plastic damage model of grouting body

In the shear test of bolted rock joints, cement slurry is used as anchorage agent. The concrete plastic damage model (CDP model) can effectively describe the mechanical behavior of brittle or quasi-brittle materials such as concrete, mortar and ceramics, as well as the failure mechanism of tensile cracking and compression crushing. Therefore, the CDP model is used to simulate the grouting body in the anchorage system. Figure 5 shows the tensile and compressive stress–strain curves under uniaxial stress state. Eq. (12) is the constitutive equation of the CDP model:

$$\left. \begin{aligned} \sigma_t &= (1 - d_t)E_0(\varepsilon_t - \bar{\varepsilon}_t^{pl}) \\ \sigma_c &= (1 - d_c)E_0(\varepsilon_c - \bar{\varepsilon}_c^{pl}) \end{aligned} \right\} \tag{12}$$

where, E_0 is the initial elastic modulus of the material; σ_t and ε_t are tensile stress and total tensile strain, respectively;

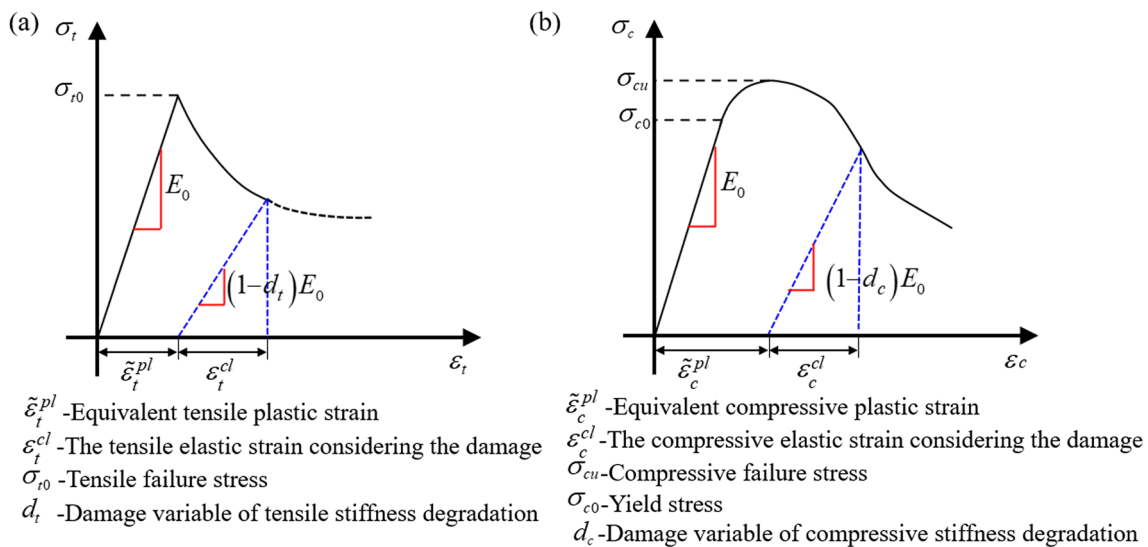


Fig. 5 Schematic diagram of tensile and compressive stress–strain relationships of CDP model under uniaxial stress

σ_c and ϵ_c are compressive stress and total compressive strain, respectively; d_c and d_t are compression damage variable and tension damage variable respectively.

3.2 Numerical simulation scheme of 2G-NPR bolt anchorage joint

According to the shear laboratory test of bolted joints, a numerical model of bolted joints is established as shown in Fig. 6. It mainly includes jointed rock mass, shear box, bolt and other solid models. The left and right sides of the upper shear box are set as fixed constraints to limit the displacement in the X direction. The normal load is applied at the top of the shear box, and the shear test under different normal stress conditions is realized by setting different load values. The tangential load is applied by setting the tangential displacement boundary condition on the side of the lower shear box. The diameter of the bolt is 8 mm, the length is 140 mm, and the length \times width \times height of the tray is 24 mm \times 24 mm \times 4 mm. The inner diameter of the grouting body is 8 mm, the outer diameter is 12 mm, and the length is 140 mm. The jointed rock mass is composed of two blocks, and the length \times width \times height of each block is 150 mm \times 150 mm \times 75 mm, and the diameter of the borehole at the center is 12 mm.

Similar to the indoor test method, in order to compare the shear resistance effect of 2G-NPR bolt, Q235 steel anchored jointed rock mass is also set up in numerical simulation. According to the indoor test, the numerical simulation model parameters mainly include rock mass, bolt and grouting body. In practical engineering, the strength of surrounding rock is complex and changeable, which has a significant influence on the anchoring performance. Therefore, in order to consider the influence of strength

Table 2 The mechanical parameters of rock mass

Rock type	Compressive strength (MPa)	Tensile strength (MPa)	Elastic modulus (GPa)	Poisson's ratio
Red-sandstone	38.52	2.97	11.2	0.26
Marble	67.64	6.66	23.5	0.24
Granite	118.45	8.09	29.8	0.21

factors such as soft rock, medium hard rock and hard rock, three types of rock mass representative of red sandstone, marble and granite are selected, and the rock mass parameters are shown in Table 2. The mechanical parameters of 2G-NPR bolt are set according to the results of Sect. 2, and the mechanical parameters of Q235 steel are shown in Table 3. The parameters of grouting body are shown in Table 4 (Zhao et al. 2022).

The eight-node hexahedron linear reduction integral solid element is adopted by bolt, grouting body and rock mass, and the rigid element is adopted by pallet and direct shear box. In order to improve the calculation accuracy, the grids near the bolt and joint surface are locally encrypted. The final number of numerical model grids is 98914, and the number of direct shear box, bolt, rock mass, grouting body and tray grids is 5520, 15138, 59104, 18576 and 576 respectively. The interface between the pallet and the two ends of the bolt is connected by tie contact, and the general contact is adopted by the other contact interfaces. The normal contact relationship is set to hard contact, and the tangential contact relationship is set to Coulomb friction model based on penalty function. Slurry bonding is used between the joint surfaces of the 2G-NPR bolt anchorage laboratory test. In the numerical simulation,

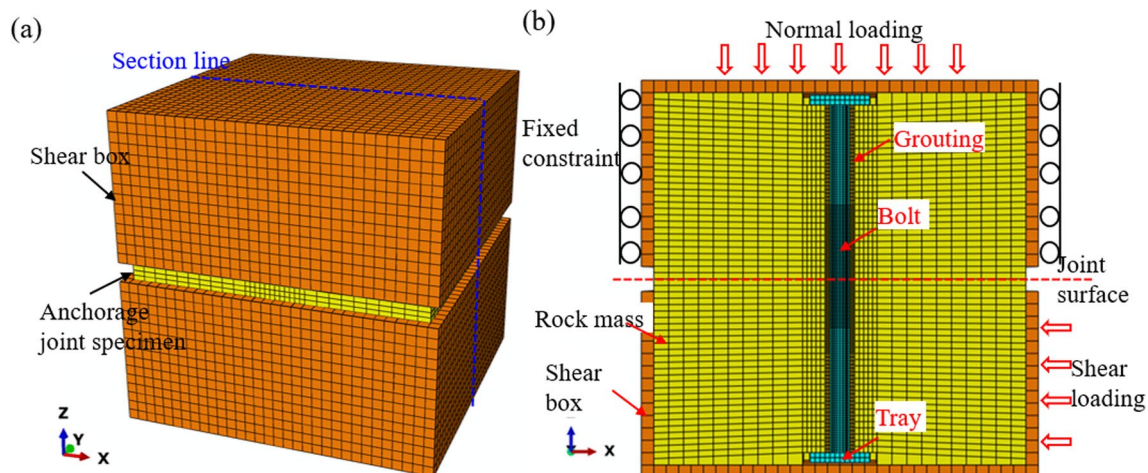


Fig. 6 Numerical calculation model of anchorage joint shear **a** Three-dimensional model diagram **b** Central profile perpendicular to the XY plane

Table 3 The mechanical parameters of Q235 steel (Zhao et al. 2022)

Bolt type	Elastic modulus (GPa)	Poisson's ratio	Yield strength (MPa)	Tensile strength (MPa)	Fracture strain	Triaxial stress	Strain ratio
Q235 steel	200	0.3	350	531	0.25	0.333	0.558

Table 4 The mechanical parameters of grouting body (Zhao et al. 2022)

Element type	Elastic modulus (GPa)	Expansion angle	Eccentricity	f_{b0}/f_{c0}	Yield constant	Viscosity coefficient
Grout	30.34	0.2	350	531	0.25	1E-005

the slurry bonding effect is simplified by increasing the friction coefficient.

4 Numerical model validation analysis

4.1 Shear simulation verification analysis of unbolted joints

The numerical simulation verification example is the shear test of unbolted marble joint surface carried out by the author (He et al. 2022). The numerical simulation results are shown in Fig. 7 under normal stress of 2 MPa, 4 MPa and 8 MPa. Similar to the curve trend of indoor test results, the simulation curve also shows the elastic rise stage, the shear force decreases after reaching the peak, and finally stabilizes in the residual stage of relatively constant shear force. The shear strength and displacement obtained by numerical simulation are in good agreement with the indoor test results. In addition, Fig. 7b shows that

the shear strength parameters of the numerical results and the experimental results are basically the same, indicating that the numerical simulation method of unanchored shear has certain reliability.

However, there are some errors between the results of numerical simulation and laboratory test, firstly, in the elastic stage of the shear force-shear displacement curve, the slope of the numerical simulation curve is larger than that of the laboratory test curve. This is mainly due to the assembly gap between the joint sample and the shear box in the laboratory test, and the inevitable millimeter-level error in the size of the sample during the processing process, which eventually leads to the difference. In addition, the indoor test curve shows the characteristics of ‘sudden drop’ of shear force after reaching the peak value, while the shear force of the numerical simulation curve decreases slightly after reaching the peak value. This is mainly due to the use of cement slurry to bond between the joint surfaces in the laboratory test. The fracture of the bond is brittle, which leads to the ‘sudden drop’ of the shear force. In order to increase the

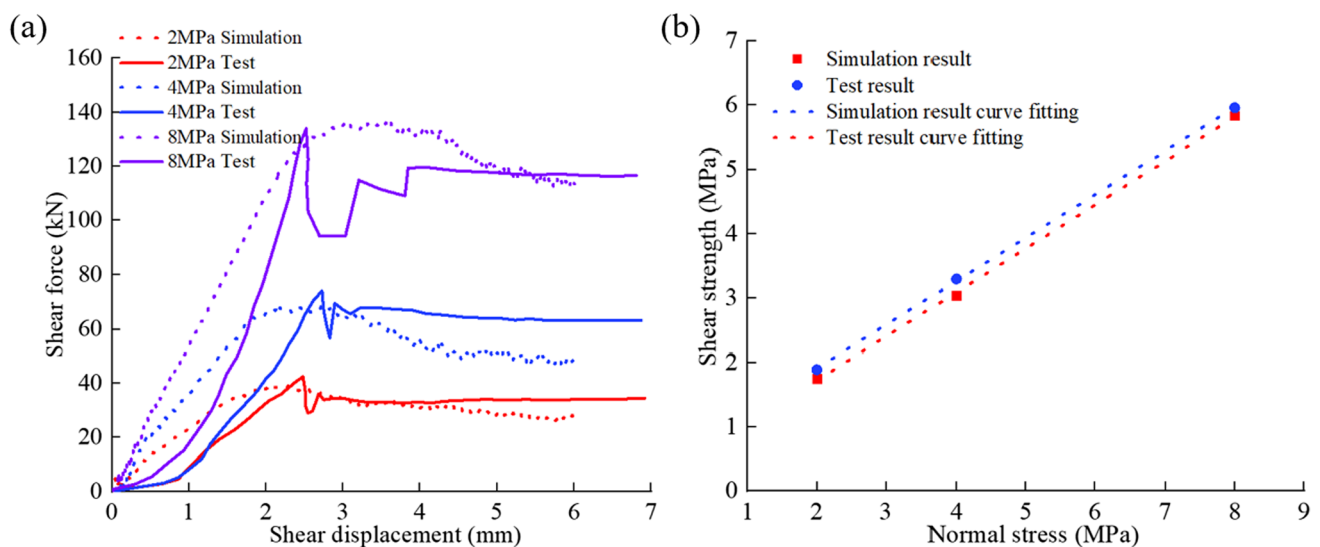


Fig. 7 Comparison of shear test and numerical results of unanchored marble joints **a** Shear force-shear displacement curve **b** Shear strength parameter fitting curve

computational efficiency in the numerical simulation, the bonding effect is simplified by increasing the friction coefficient. Only the friction between the joint surfaces is considered, and the bonding effect is not considered, which leads to the difference between the indoor test and the numerical simulation.

4.2 Shear simulation verification analysis of bolted joints

The numerical simulation of anchorage joints is also verified by the test results in the literature (He et al. 2022).

4.2.1 Verification analysis of bolt deformation and failure

As shown in Fig. 8, under the condition of normal stress of 2 MPa, when the shear displacement is 30 mm, the stress distribution diagram at the XZ center section of the anchored red sandstone joint and granite joint. The bolt shows ‘S’-shaped deformation characteristics along the joint surface. Under the same conditions, the anchoring shear resistance of 2G-NPR bolt is significantly better than that of Q235 steel. Under the condition of anchoring red sandstone joints, Q235 steel fractured at the joint surface, while 2G-NPR bolt did not fracture. In addition, with the increase of rock strength,

Q235 steel and 2G-NPR bolt show the characteristics of decreasing shear deformation resistance. The numerical simulation results of the shear deformation failure characteristics of the bolt are in good agreement with the indoor test results. This simulation method can effectively show the shear deformation behavior of the bolt anchorage test under different surrounding rock strength conditions.

4.2.2 Verification analysis of deformation and failure of jointed rock mass

Figure 9 shows the stress distribution and plastic zone distribution of 2G-NPR bolt anchored red sandstone joints when the shear displacement is 5.620 mm. Figure 9a is the stress distribution map of the XZ central section of the jointed rock mass. Under the action of shear load, the rock mass is squeezed by the bolt and the rock mass forms a central symmetrical compressive stress zone at the intersection of the joint surface and the bolt. The plastic zone distribution of the XZ center section of the jointed rock mass in Fig. 9b shows that the rock mass gradually forms a plastic zone in the compressive stress zone, that is, the rock mass is destroyed. In addition, due to the bending deformation of the bolt during the shearing process, the tensile zone is formed on the other side of the bolt in the compression zone of the

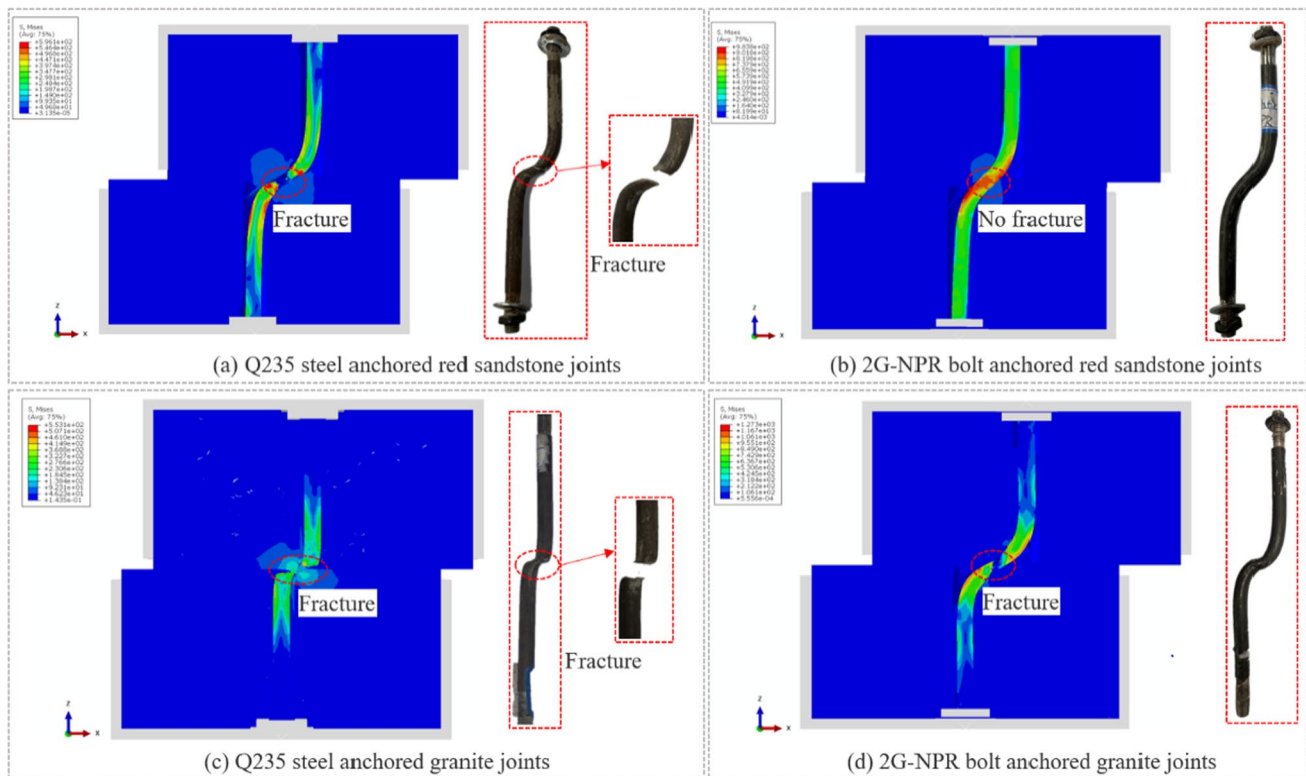


Fig. 8 Comparison of deformation and failure characteristics between numerical simulation of anchorage shear and laboratory test (normal stress 2 MPa, shear displacement 30 mm)

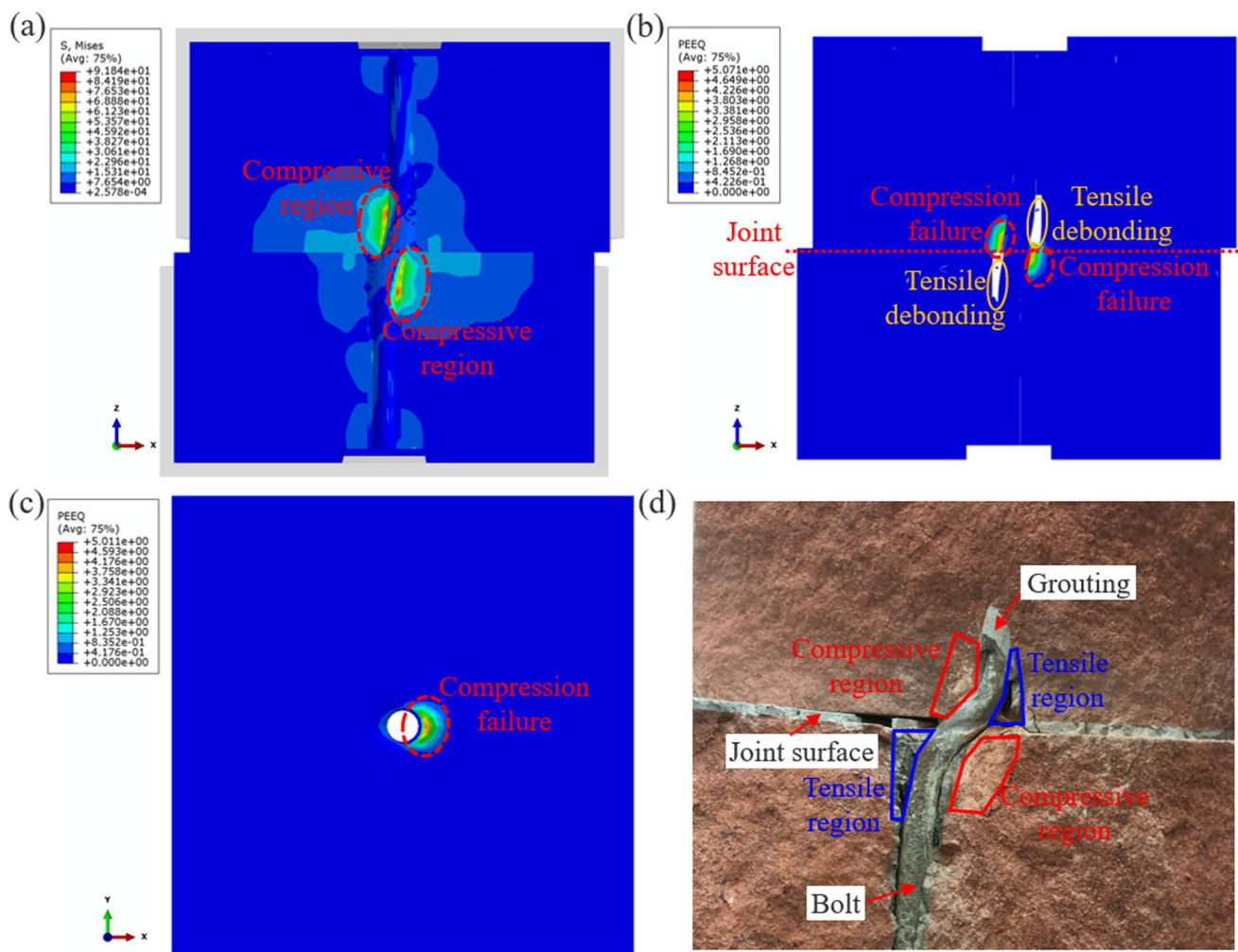


Fig. 9 Comparison between numerical simulation and laboratory test results of 2G-NPR bolt anchored red sandstone joints **a** Stress distribution diagram of XZ central section of jointed rock mass **b** Plastic

distribution diagram of XZ central section of jointed rock mass **c** Plastic distribution diagram of footwall jointed rock mass **d** Laboratory test results (He et al. 2022)

rock mass. The remarkable feature is that the grouting body in the tensile zone is first subjected to tensile failure, and the debonding between the bolt and the rock mass occurs to form a tensile zone. Figure 9c shows the distribution of plastic zone on XY plane of footwall jointed rock mass, and plastic failure occurs on one side of rock mass hole due to bolt pressure. Figure 9d shows the indoor test results under this working condition. The numerical simulation results are in good agreement with the test results. The simulation method can effectively reflect the deformation characteristics and failure behavior of jointed rock mass during anchorage shear process.

The results of the shear force-shear displacement curve of the anchorage shear test can intuitively reflect the effect of the bolt on the deformation and strength improvement of the jointed rock mass, as shown in the comparison of the curve results of numerical simulation and laboratory test.

Figure 10a shows the numerical simulation and laboratory test results of 2G-NPR bolt anchored red sandstone joints under normal stress of 2 MPa. Due to the limitation of the range of indoor shear test, the 2G-NPR bolt failed to break during the experiment under this working condition, and the fracture displacement and shear strength of 2G-NPR bolt anchored red sandstone joints could not be obtained. The numerical simulation method can make up for this deficiency. By setting a larger shear displacement termination condition, the fracture displacement and shear strength under this working condition are finally obtained. Figure 10b shows the numerical simulation and laboratory test results of 2G-NPR bolt anchored granite joints under normal stress of 4 MPa. The two have good consistency in fracture displacement, shear resistance and overall curve characteristics.

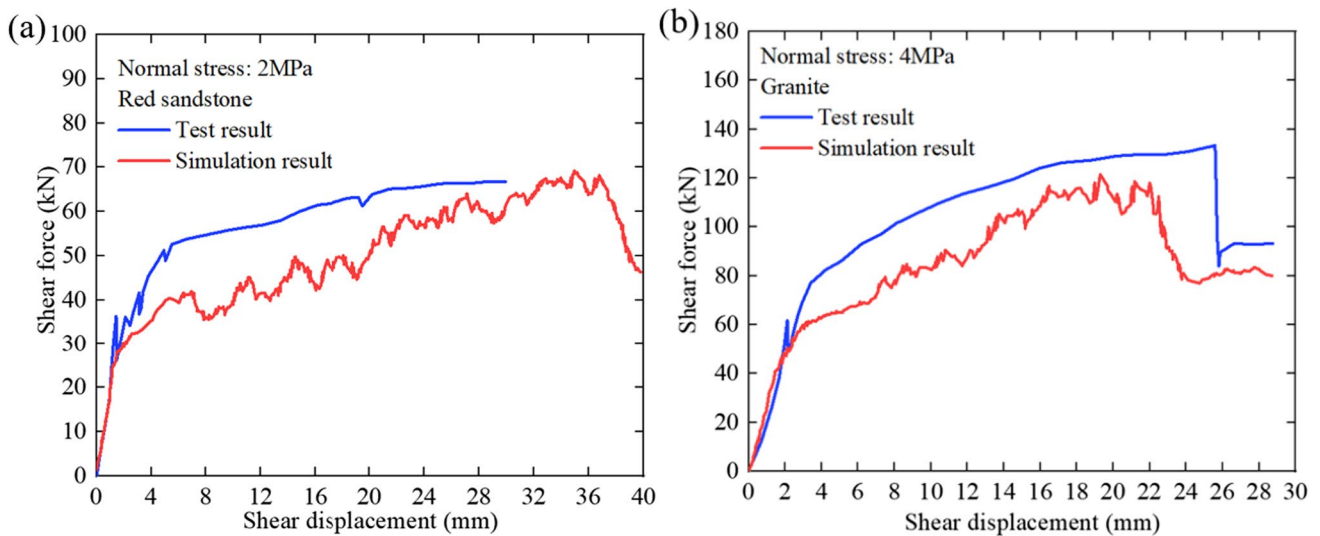


Fig. 10 Comparison of results of laboratory test and numerical simulation on the shear force–shear displacement curve of 2G-NPR bolt **a** Red sandstone joint, 2 MPa normal stress **b** Granite joint, 4 MPa normal stress

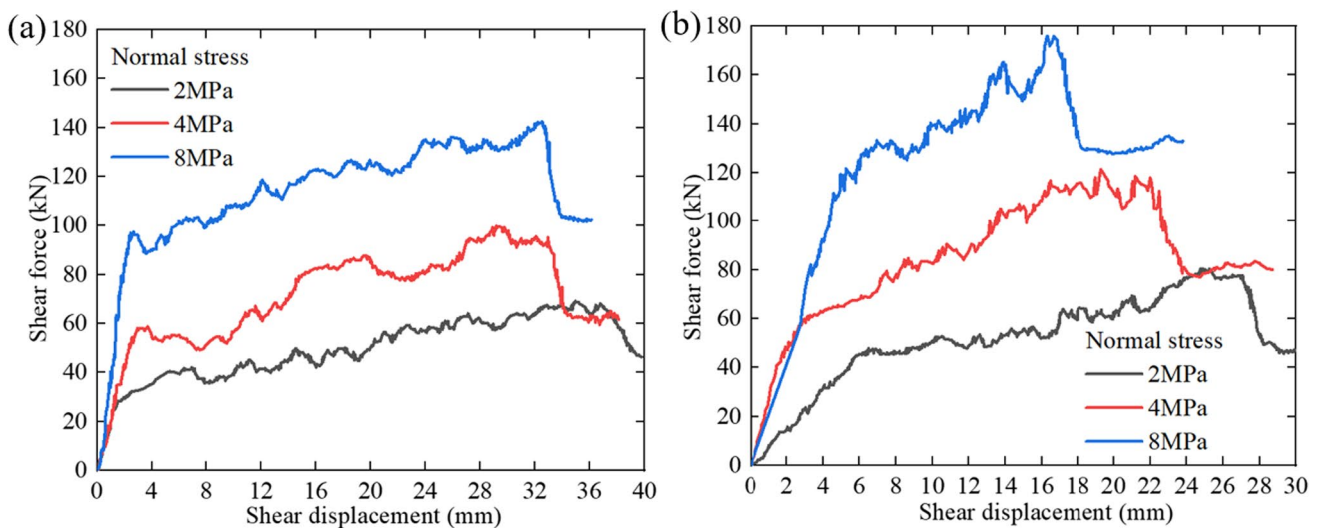


Fig. 11 Simulation results of 2G-NPR bolt shear force–shear displacement curve **a** Red sandstone joints **b** Granite joints

Figure 11a and b are the results of shear force–shear displacement curves of red sandstone joints and granite joints bolted by 2G-NPR bolts under normal stress conditions of 2, 4 and 8 MPa, respectively. With the increase of normal stress, the shear strength increases, and the Mohr–Coulomb criterion is satisfied. In addition, the anchorage shear displacement shows a decreasing trend, which is consistent with the indoor test results.

Based on the comprehensive analysis of the results of numerical simulation and laboratory test curves, because the initial bonding effect between joint surfaces is not considered in the numerical simulation, the curve drop

characteristics caused by the failure of bonding effect are not shown in the simulation results, but the simplification of this condition does not affect the study of key parameters such as shear displacement and shear force of bolt anchorage shear curve. The results of the numerical simulation curve also have the characteristics of the initial elastic stage, the yield stage, the plastic strengthening stage and the fracture stage. However, due to the simplification of some conditions in the numerical simulation, such as the damage and crushing of the surrounding rock, and some errors in the indoor test, such as the installation gap between the shear box and the anchored rock mass, the

processing size error of the rock sample, etc., the characteristic parameters such as shear displacement and shear strength have small differences. In general, the numerical simulation results are in good agreement with the laboratory test results.

4.3 Analysis of shear simulation results of bolted joints

The indoor test of anchorage shear is limited by monitoring instruments, which makes it impossible to effectively monitor and analyze the stress–strain evolution, deformation behavior of bolt and grouting body in the shear process of anchorage shear system. Numerical simulation can effectively solve this problem. On the basis of verifying

the accuracy of numerical simulation, the numerical simulation method is used to analyze the stress and strain of bolt and the deformation behavior of grouting body, which plays an important role in perfecting the indoor test data and revealing the mechanism of anchorage shear resistance.

4.3.1 Stress field analysis of bolt

Figure 12 is the maximum principal stress distribution map of 2G-NPR bolt and Q235 steel anchored granite joints during shearing under normal stress of 2 MPa. The results show that the bolt presents similar stress distribution characteristics in the process of anchoring shear resistance. Under the mutual restraint of surrounding rock,

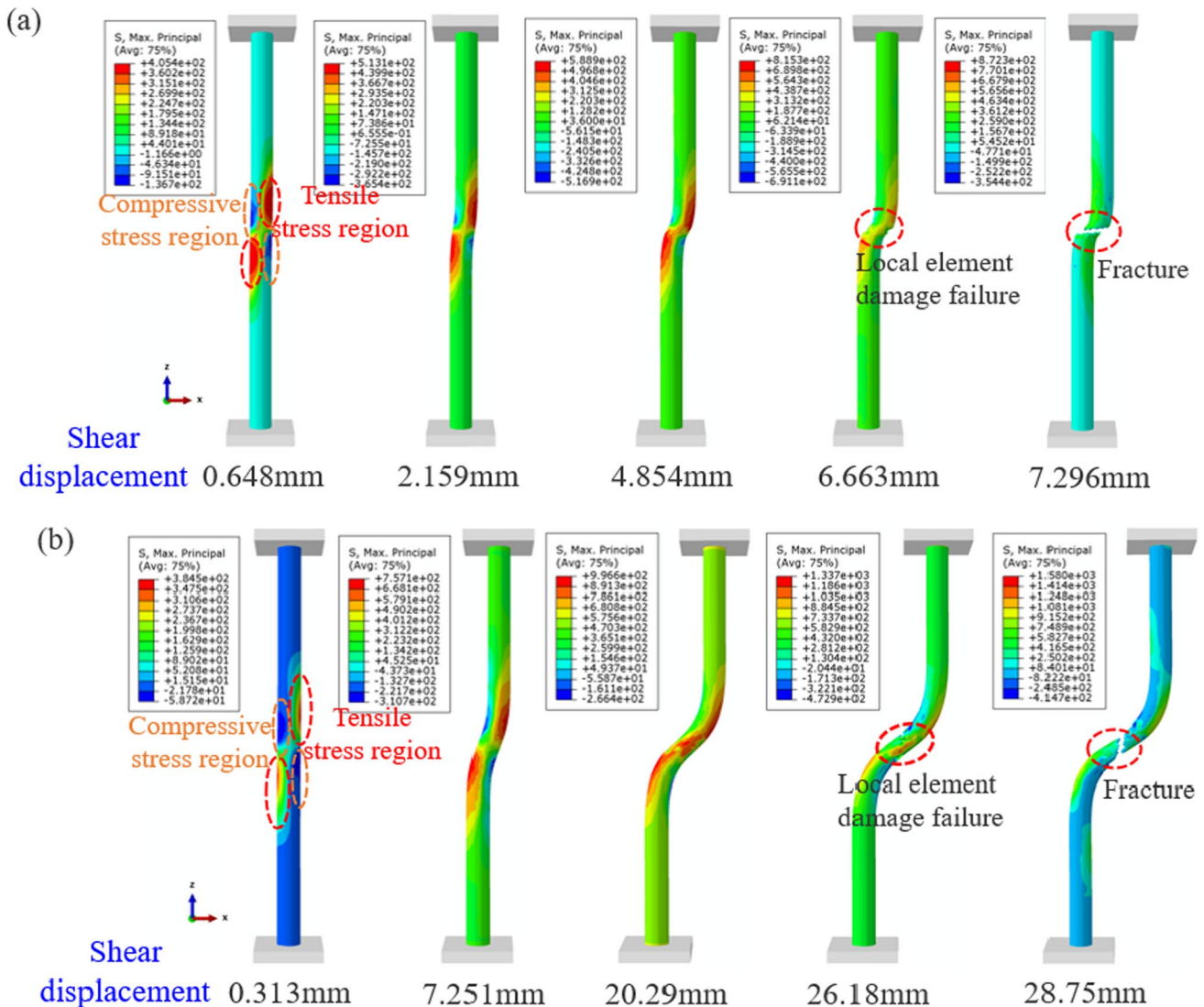


Fig. 12 Maximum principal stress distribution of bolt during anchorage shear **a** Granite joint anchored by Q235 steel **b** Granite joint anchored by 2G-NPR bolt

the bolt forms compressive stress zone and tensile stress zone at the joint surface, and the bolt presents ‘S’ shape deformation characteristics. The bolt forms plastic hinges on both sides of the joint surface, and the geometric feature is that the bolt bends to form the maximum curvature point. With the gradual increase of shear displacement, the stress of the bolt is mainly concentrated in the transverse deformation zone of the bolt between the plastic hinges. When the peak displacement is about to reach, the local element at the junction of the bolt and the joint surface is damaged, and then the fracture failure occurs.

Under the same test conditions, the stress in the tensile and compressive stress zone of 2G-NPR bolt is significantly higher than that of Q235 steel at each stage of anchorage shear, which ultimately leads to the higher anchorage shear strength of 2G-NPR bolt than that of Q235 steel.

4.3.2 Stress–strain analysis of bolt

In order to further study the axial and tangential deformation characteristics and mechanical behavior of bolt anchorage, the axial stress and shear stress of bolt are monitored and analyzed. Figure 13 is a cross-section diagram of the bolt along the XZ axis. The position relationship of the monitoring points is defined from the top to the bottom of the axial direction of the bolt. The top is the coordinate 0 point. The length of the numerical simulation bolt is 140 mm, so the axial position of the bottom is 140 mm, and the joint surface is 70 mm. The Path monitoring path of Abaqus is used to monitor the relationship between stress and strain and axial position during the shear test. The right side of the bolt section is the A-side monitoring path, and the left side is the B-side monitoring path.

Figure 14 is the stress monitoring result curve of bolt A side and B side when the shear displacement of 2G-NPR bolt anchored red sandstone joint is 2.420 mm and 6.016 mm under the normal stress of 2 MPa. The results show that the axial stress and shear stress on the A and B sides of the bolt are antisymmetric along the intersection of the bolt and the joint surface. The compressive stress of the bolt is negative and the tensile stress is positive. The axial force of the compressive side is significantly higher than that of the tensile side, and the axial force of the bolt at the joint surface is the lowest. The shear stress distribution curve shows that the

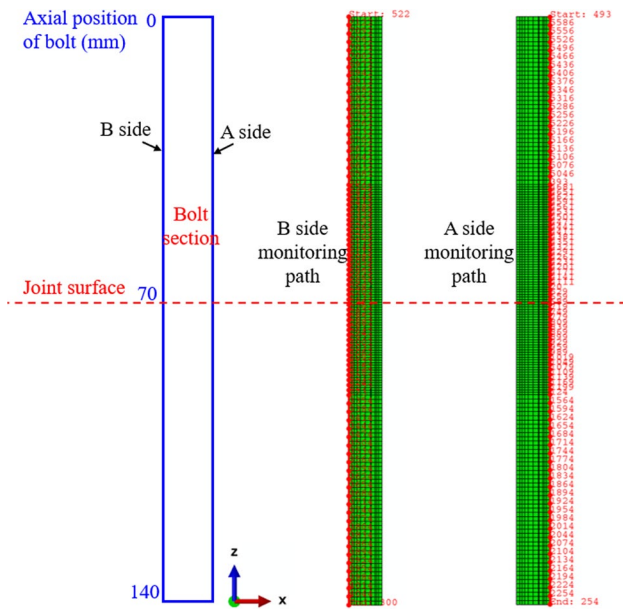


Fig. 13 Schematic diagram of bolt monitoring section

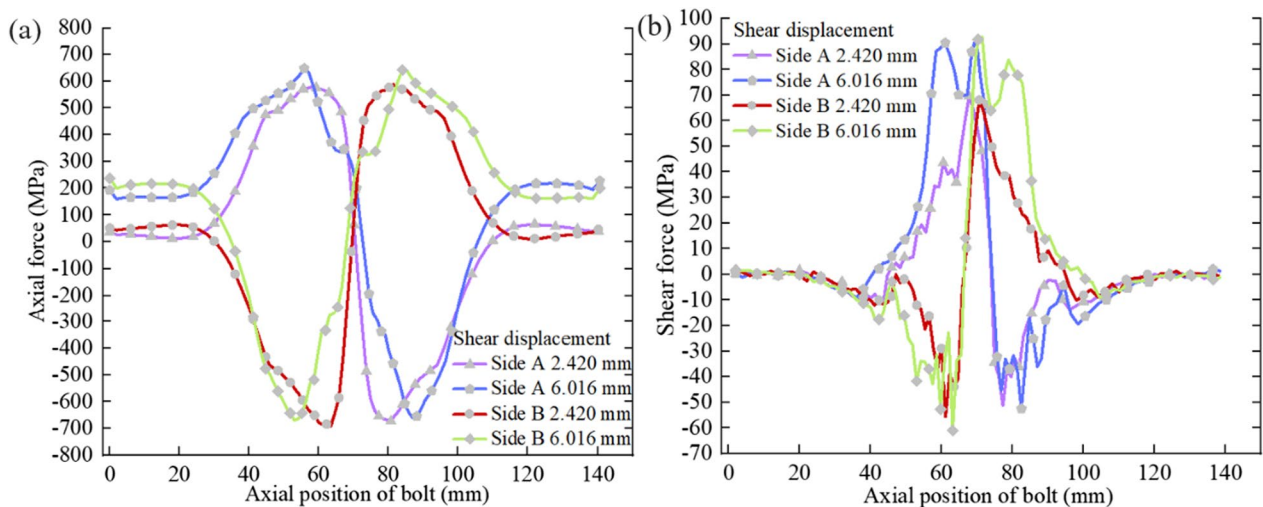


Fig. 14 Monitoring results of the left and right side stress of the bolt monitoring section a Monitoring results of axial force b Monitoring results of shear force

shear stress of the bolt is the largest at the joint surface, and the shear force on the compression side is lower than that on the tension side. The shear stress distribution gradually decreases along the axial direction of the two ends of the bolt. After reaching a critical position, the shear stress is basically 0, which is the boundary point between the elastic deformation and plastic deformation of the anchorage shear, and also the main area where the bolt plays the role of shear.

Based on the anti-symmetric distribution characteristics of the monitoring sections on the left and right sides of the bolt, the subsequent stress–strain analysis only shows and analyzes the monitoring results on the A side. Figure 15 shows the monitoring curve results of axial force and shear force of 2G-NPR bolt anchored red sandstone joints from the initial stage of shear load loading to bolt fracture under normal stress of 2 MPa. The axial force of the bolt at the joint surface is basically 0. As the shear displacement increases, the axial force of each part of the bolt tends to increase. The axial force of the bolt on both sides of the joint surface is divided into compressive stress and tensile stress distribution characteristics. The axial force of the bolt on the loaded side is negative, mainly bearing compressive stress, while the axial force at both ends of the bolt is mainly tensile. When the shear displacement is 35.08 mm, the bolt is about to break, and the axial compressive stress of the bolt develops into the axial tensile stress state, which finally causes the bolt to break. Figure 15b is the shear force distribution map of the bolt at different axial positions. The shear force of the bolt at the joint surface is the largest, and the shear force at both ends of the bolt is 0 in a certain range. With the increase of shear displacement, the shear force of bolt increases and the range of shear zone increases gradually.

In order to compare and analyze the anchorage shear stress and strain characteristics of 2G-NPR bolt and Q235 steel, Fig. 16 shows the axial force and shear force distribution of 2G-NPR bolt and Q235 steel anchored granite joints under normal stress of 2 MPa. The fracture point of Q235 bolt is reached when the shear displacement is 6.641 mm, while the fracture shear displacement of 2G-NPR bolt is 25.86 mm. Under the same shear displacement condition, the axial force of 2G-NPR bolt is significantly higher than that of Q235 steel, indicating that 2G-NPR bolt can provide higher shear strength. The shear stress distribution diagram shows that the shear range of 2G-NPR bolt is significantly higher than that of Q235 steel, indicating that the interaction range between 2G-NPR bolt and surrounding rock is larger, which can provide higher shear strength and shear deformation capacity for the anchorage shear of jointed rock mass.

4.3.3 Deformation and failure analysis of grouting body

Figure 17 shows the stress distribution map of deformation and failure of 2G-NPR bolt anchored red sandstone joint grouting body under normal stress of 2 MPa. In order to further explore the failure characteristics of the grouting body, a stiffness reduction coefficient of the grouting body element is set in the CDP constitutive model, which deletes the elements with high degree of damage and deterioration according to the strain of the element. In the early stage of shear loading, obvious compressive stress zone and tensile stress zone are formed along both sides of the joint surface, and the shear stress at the joint surface is the largest. The grouting body has obvious brittle damage and failure characteristics. The unit is damaged under the condition of

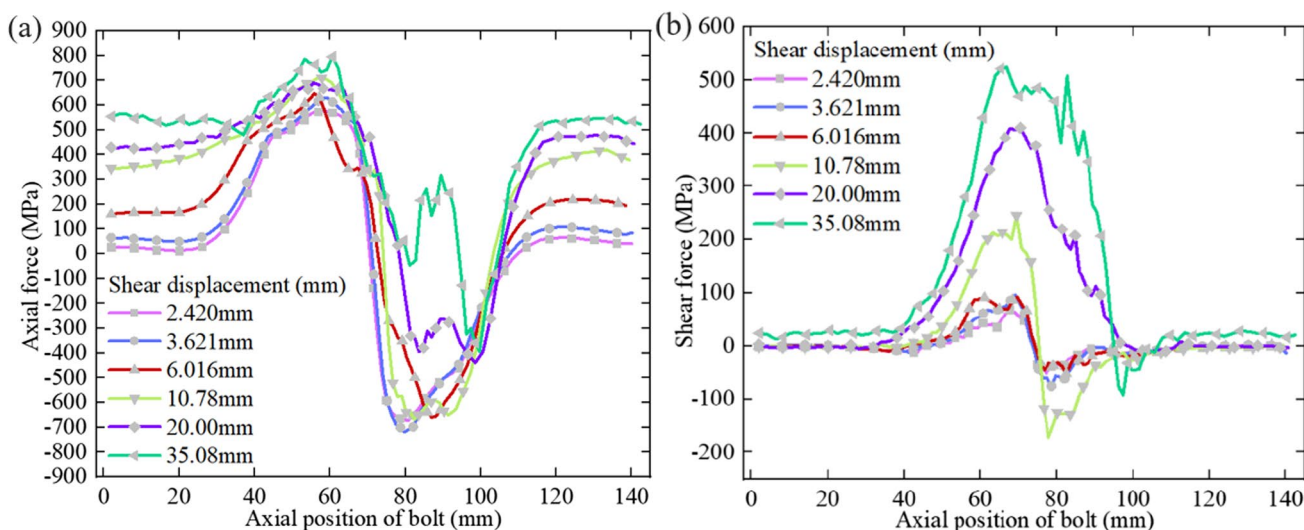


Fig. 15 Stress–strain monitoring results of red sandstone joints anchored by 2G-NPR bolt a Axial force b Shear force

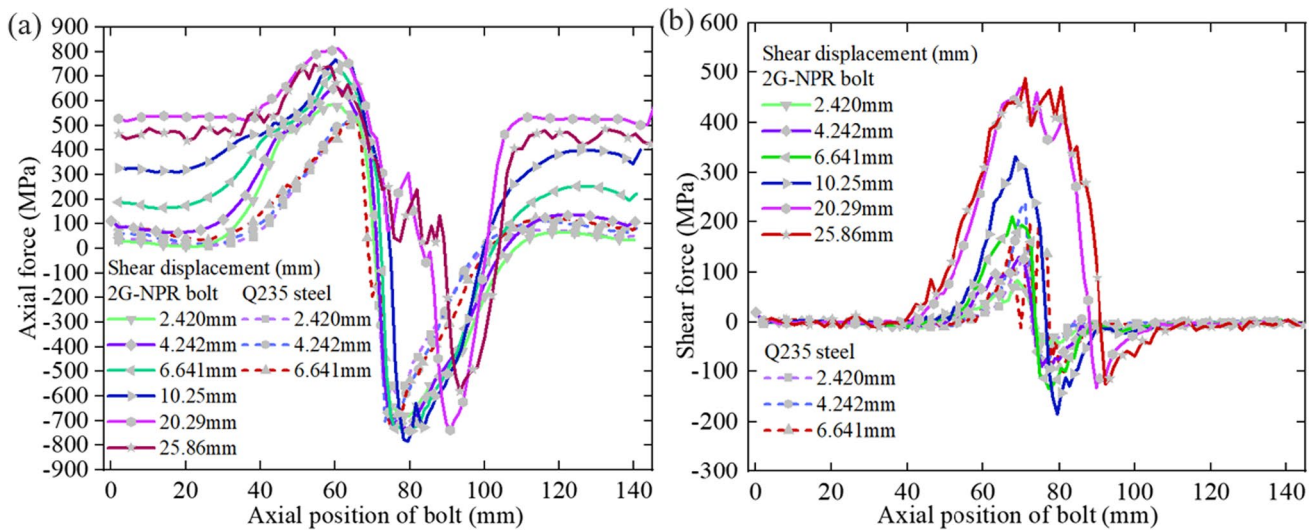


Fig. 16 Stress–strain monitoring results of 2G-NPR bolt and Q235 steel anchorage granite joint bolt a Axial force b Shear force

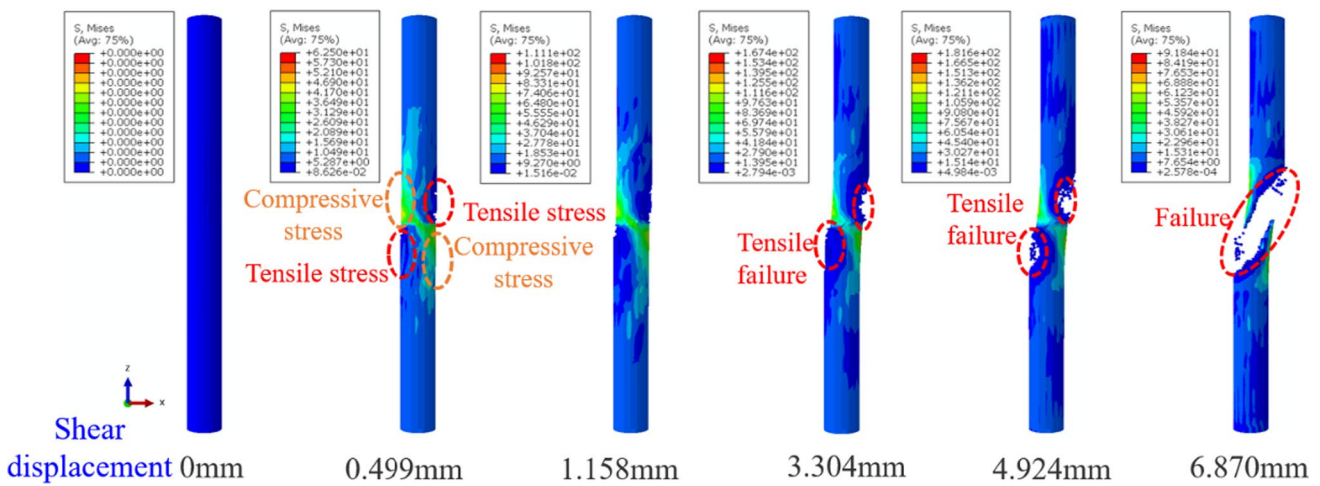


Fig. 17 Stress evolution characteristics of joint grouting body of red sandstone anchored by 2G-NPR bolt

small shear displacement. When the shear displacement is 4.924 mm, the macroscopic tensile failure occurs first in the tensile zone of the grouting body. With the further increase of shear displacement, when it reaches 6.870 mm, brittle failure occurs in the tensile zone of grouting body on both sides of joint surface, and the bonding effect of grouting body fails. Therefore, the bonding effect of the grouting body on the transverse shear deformation zone of the bolt only plays a certain role in the initial stage of shear load loading. When the large shear deformation occurs, the grouting body itself is completely destroyed, and the shear effect is mainly exerted by the bolt itself.

5 Conclusions

- (1) The indoor mechanical tests of 2G-NPR bolt under different tensile–shear angles were carried out. The results show that the mechanical curve of 2G-NPR bolt has no yield platform and has a large uniform deformation elongation ability, showing quasi-ideal elastic–plastic mechanical characteristics. As the tensile–shear angle increases, its mechanical deformation performance gradually decreases. Based on the weighted average method and finite element analysis method, the true stress–strain curve of 2G-NPR bolt with full loading

history was obtained. The average stress triaxiality and fracture strain of NRP bolt were fitted by Johnson–Cook fracture criterion, and the fracture prediction model of 2G-NPR bolt under tensile–shear test conditions was established.

- (2) A three-dimensional refined numerical simulation method for the shear behavior of anchored rock joints is proposed, which comprehensively considers the elastic–plastic mechanical behavior of rock mass, the constitutive fracture criterion of bolt tension–shear mechanics and the damage and deterioration of grouting body. Compared with the indoor test results under different surrounding rock strength and normal stress conditions, the validity and accuracy of the numerical method are verified from the aspects of shear force–shear displacement curve and macroscopic deformation and failure characteristics.
- (3) The stress field evolution characteristics of bolt and grouting body in the process of shear resistance of anchorage joint are analyzed. The grouting body only plays a certain role in the initial stage of shear load loading. When the anchorage system undergoes large shear deformation, the grouting body itself undergoes a more macroscopic failure, mainly by the bolt itself. The bolt forms compressive stress zone and tensile stress zone on both sides of the joint surface. The shear force of the bolt at the joint surface is the largest, and the axial force of the bolt is basically 0. Under the same shear displacement condition, the stress in the tensile and compressive stress zone of 2G-NPR bolt is significantly higher than that of Q235 steel. In addition, the interaction range between 2G-NPR bolt and surrounding rock is larger, which can provide higher shear strength and shear deformation ability for anchorage shear resistance of jointed rock mass.

Acknowledgements This work described herein was supported by the National Natural Science Foundation of China (NSFC) (41941018).

Author contributions SR: Methodology, Investigation, Software, Validation, Formal analysis, Writing—original draft, Writing—review & editing. ZT: Project administration, Methodology, Formal analysis. MH: Conceptualization, Resources, Supervision, Funding acquisition. ML: Investigation. QS: Investigation.

Declarations

Conflict of interest The authors declare that they have no known conflict of interest or personal relationships that could have appeared to influence the work reported in this paper.

Open Access This article is licensed under a Creative Commons Attribution 4.0 International License, which permits use, sharing, adaptation, distribution and reproduction in any medium or format, as long as you give appropriate credit to the original author(s) and the source, provide a link to the Creative Commons licence, and indicate if changes

were made. The images or other third party material in this article are included in the article's Creative Commons licence, unless indicated otherwise in a credit line to the material. If material is not included in the article's Creative Commons licence and your intended use is not permitted by statutory regulation or exceeds the permitted use, you will need to obtain permission directly from the copyright holder. To view a copy of this licence, visit <http://creativecommons.org/licenses/by/4.0/>.

References

- Bjurstrom S (1974) Shear strength of hard rock joints reinforced by grouted untensioned bolts. In: *Advances in rock mechanics: proceedings of the 3rd congress of the international society for rock mechanics*. National Academy of Sciences, Washington, pp 1194–1199
- Chen Y (2014) Experimental study and stress analysis of rock bolt anchorage performance. *J Rock Mech Geotech* 6(5):428–437
- Chen Y, Li CC (2015) Performance of fully encapsulated rebar bolts and D-Bolts under combined pull-and-shear loading. *Tunn Undergr Space Technol* 45:99–106
- Chen N, Zhang XB, Jiang QH et al (2018) Shear behavior of rough rock joints reinforced by bolts. *Int J Geomech* 18(1):04017130
- Chen Y, Lin H, Xie S et al (2022) Effect of joint microcharacteristics on macroshear behavior of single-bolted rock joints by the numerical modelling with PFC. *Environ Earth Sci* 81:276
- Cui GJ, Zhang CQ, Chen JL et al (2020) Effect of bolt inclination angle on shear behavior of bolted joints under CNL and CNS conditions. *J Cent South Univ* 27(3):937–950
- Grasselli G (2005) 3D behaviour of bolted rock joints: experimental and numerical study. *Int J Rock Mech Min Sci* 42(1):13–24
- Gu TY, Jia LJ, Chen B et al (2021) Unified full-range plasticity till fracture of meta steel and structural steels. *Eng Fract Mech* 10:107869
- He MC, Wang Q, Wu Q (2021) Innovation and future of mining rock mechanics. *J Rock Mech Geotech* 13(9):1–21
- He MC, Ren SL, Guo LJ et al (2022) Experimental study on influence of host rock strength on shear performance of Micro-NPR steel bolted rock joints. *Int J Rock Mech Min Sci* 159:105236
- He MC, Ren SL, Xu HT et al (2023) Experimental study on the shear performance of quasi-NPR steel bolted rock joints. *J Rock Mech Geotech* 15:350–362
- Jalalifar H, Aziz N (2010) Analytical behaviour of bolt–joint intersection under lateral loading conditions. *Rock Mech Rock Eng* 43(1):89–94
- Jalalifar H, Aziz N, Hadi M (2006) The effect of surface profile, rock strength and pretension load on bending behaviour of fully grouted bolts. *Geotech Geolog Eng* 24(5):1203–1227
- Jia LJ, Zhang R, Zhou CF et al (2023) In-situ three-dimensional X-ray investigation on micro ductile fracture mechanism of a high-Mn steel with delayed necking effect. *J Mater Res Technol* 24:1076–1087
- Jiang Y, Zhang S, Luan H et al (2022) Numerical modelling of the performance of bolted rough joint subjected to shear load. *Geomech Geophys Geo-Energ Geo-Resour* 8(5):1–21
- Johnson GR, Cook WH (1985) Fracture characteristics of three metals subjected to various strains, strain rates, temperatures and pressures. *Eng Fract Mech* 21(1):31–48
- Li CC (2010a) Field observations of rock bolts in high stress rock masses. *Rock Mech Rock Eng* 43(4):491–496
- Li CC (2010b) A new energy-absorbing bolt for rock support in high stress rock masses. *Int J Rock Mech Min Sci* 47(3):396–404
- Li YZ, Liu CH (2019) Experimental study on the shear behavior of fully grouted bolts. *Constr Build Mater* 223:1123–1134
- Li XW, Nemeik J, Mirzaghobanali A et al (2015) Analytical model of shear behaviour of a fully grouted cable bolt subjected to shearing. *Int J Rock Mech Min Sci* 80:31–39

- Li X, Aziz N, Mirzaghobanali A et al (2016) Behavior of fiber glass bolts, rock bolts and cable bolts in shear. *Rock Mech Rock Eng* 49(7):2723–2735
- Lin H, Xiong Z, Liu T et al (2014) Numerical simulations of the effect of bolt inclination on the shear strength of rock joints. *Int J Rock Mech Min Sci* 66:49–56
- Ling Y (1996) Uniaxial true stress-strain after necking. *AMP J Tech* 5
- Liu CH, Li YZ (2017) Analytical study of the mechanical behavior of fully grouted bolts in bedding rock slopes. *Rock Mech Rock Eng* 50(9):2413–2423
- Ma S, Zhao Z, Shang J (2019) An analytical model for shear behaviour of bolted rock joints. *Int J Rock Mech Min Sci* 121:104019
- Saadat M, Taheri A (2019) Effect of contributing parameters on the behaviour of a bolted rock joint subjected to combined pull-and-shear loading: a DEM approach. *Rock Mech Rock Eng* 53:383–409
- Singh P, Spearing AJS, Jessu K (2020) Analysis of the combined load behaviour of rock bolt installed across discontinuity and its modeling using FLAC3D. *Geotech Geol Eng* 38(6):5867–5883
- Song YB, Yan S, Bai JB et al (2017) Implementation of shear broken failure of bolts in FLAC3D and its application. *China J Rock Mech Eng* 36(8):1899–1909
- Song Y, Wang J, Uy B et al (2020) Experimental behaviour and fracture prediction of austenitic stainless steel bolts under combined tension and shear. *J Constr Steel Res* 166:105916
- Tang J, He MC, Qiao YF et al (2021) Tensile behavior of a novel high-strength and high-toughness steel at strain rates from 0.1 s^{-1} to 1000 s^{-1} . *Constr Build Mater* 304(12):124606
- Wu X, Jiang Y, Li B (2018) Influence of joint roughness on the shear behaviour of fully encapsulated rock bolt. *Rock Mech Rock Eng* 51:953–959
- Wu X, Jiang Y, Gong B et al (2019a) Shear performance of rock joint reinforced by fully encapsulated rock bolt under cyclic loading condition. *Rock Mech Rock Eng* 52:2681–2690
- Wu X, Jiang Y, Wang G et al (2019b) Performance of a new yielding rock bolt under pull and shear loading conditions. *Rock Mech Rock Eng* 52(9):3401–3412
- Zhang XW, Wen JF, Zhang XC et al (2019) Effects of the stress state on plastic deformation and ductile failure: Experiment and numerical simulation using a newly designed tension-shear specimen. *Fatigue Fract Eng Mater Struct* 42(9):2079–2092
- Zhang YC, Jiang YJ, Wang Z et al (2022) Anchorage effect of bolt on en-echelon fractures: a comparison between energy-absorbing bolt and conventional rigid bolt. *Eng Fail Anal* 137:106256
- Zhao ZH, Liu H, Sun W et al (2022) Progressive damage and failure behavior of rock-mass anchorage system considering interface effect. *Rock Soil Mech* 43(11):3163–3173
- Zheng L, Wang L, Zhu L et al (2021) Analytical model of the shear behaviors of bolted rough joints based on the dilation effect and surface abrasion. *Eng Geol* 294:106399

Publisher's Note Springer Nature remains neutral with regard to jurisdictional claims in published maps and institutional affiliations.